Carderock Division
Naval Surface Warfare Center
West Bethesda, Maryland 20817-5700

NSWCCD-50-TR-2008 / 061 August 2008
Hydromechanics Department Report

Measurement of Crashback Loads on a Blade of Propeller 4381 in an Open and Ducted Configuration in the 36-inch Water Tunnel

by

Susan B. Swithenbank
Stuart Jessup
Ali Etebari

NSWCCD-50-TR-2008/061 Measurement of Crashback Loads on a Blade of Propeller 4381 in an Open and Ducted Configuration in the 36-inch Water Tunnel

Carderock Division
Naval Surface Warfare Center
West Bethesda, Maryland 20817-5700

NSWCCD-50-TR-2008 / 061 August 2008
Hydromechanics Department Report

Measurement of Crashback Loads on a Blade of Propeller 4381 in an Open and Ducted Configuration in the 36-inch Water Tunnel

by

Susan B. Swithenbank
Stuart Jessup
Ali Etebari

NSWCCD-50-TR-2008/061 Measurement of Crashback Loads on a Blade of Propeller 4381 in an Open and Ducted Configuration in the 36-inch Water Tunnel

REPORT DOCUMENTATION PAGE

Form Approved OMB No. 0704-0188

1. REPORT DATE *(DD-MM-YYYY)*	2. REPORT TYPE	3. DATES COVERED *(From - To)*
08/08/2008	Technical	Feb. 2008 to Aug. 2008

4. TITLE AND SUBTITLE
Measurement of Crashback Loads on a Blade of Propeller 4381 in an Open and Duted Configuration in the 36-inch Water Tunnel

5a. CONTRACT NUMBER

5b. GRANT NUMBER

5c. PROGRAM ELEMENT NUMBER

6. AUTHOR(S)
Susan B. Swithenbank, Stuart Jessup, and Ali Etebari

5d. PROJECT NUMBER

5e. TASK NUMBER

5f. WORK UNIT NUMBER

7. PERFORMING ORGANIZATION NAME(S) AND ADDRESS(ES) AND ADDRESS(ES)

Naval Surface Warfare Center
Carderock Division
9500 Macarthur Boulevard
West Bethesda, MD 20817-5700

8. PERFORMING ORGANIZATION REPORT NUMBER

NSWCCD-50-TR-2008/061

9. SPONSORING / MONITORING AGENCY NAME(S) AND ADDRESS(ES)

Code 5080
NSWCCD

Office of Naval Research
875 North Randolph St.
Arlington, VA 22203

10. SPONSOR/MONITOR'S ACRONYM(S)

11. SPONSOR/MONITOR'S REPORT NUMBER(S)

12. DISTRIBUTION / AVAILABILITY STATEMENT
Approved for public release. Distribution unlimited.

13. SUPPLEMENTARY NOTES

14. ABSTRACT

Propeller 4381 was tested in crashback conditions in the 36-inch water tunnel at the Naval Surface Warfare Center, Carderock Division. The propeller was tested in both an open and ducted configuration to look at the differences in strain and derived bending moment loads at the root of a blade. Time history measurements were analyzed to determine unsteady strain levels at the root of the blade. The maximum unsteady strains were up to 2.5 times the mean strain on the blade for both configurations. The open and ducted configuration had similar maximum strain components, but the mean strain was lower for the ducted cases at advance coefficient values between -0.2 and -0.7.

15. SUBJECT TERMS

16. SECURITY CLASSIFICATION OF:			17. LIMITATION OF ABSTRACT	18. NUMBER OF PAGES	19a. NAME OF RESPONSIBLE PERSON
a. REPORT	b. ABSTRACT	c. THIS PAGE			Susan B Swithenbank
UNCLASSIFIED	UNCLASSIFIED	UNCLASSIFIED	SAR	29+iv	19b. TELEPHONE NUMBER (301) 227-5839

THIS PAGE INTENTIONALLY LEFT BLANK

Contents

Figures

Tables

Nomenclature

c – chord
D – diameter (ft.)
F – camber
J – advance coefficient V/nD
K_T – thrust coefficient $T/\rho n^2 D^4$
M – bending moment at root
n – propeller rotational speed (rps)
P – pitch
r – radius
R – propeller tip radius
t – thickness
T – thrust (lbs.)
V – tunnel velocity (ft/s)
ρ – density

Abstract

Propeller 4381 was tested in crashback conditions in the 36-inch water tunnel at the Naval Surface Warfare Center, Carderock Division. The propeller was tested in both an open and ducted configuration to look at the differences in strain and derived bending moment loads at the root of a blade. Time history measurements were analyzed to determine unsteady strain levels at the root of the blade. The maximum unsteady strains were at up to 2.5 times the mean strain on the blade for both configurations. The open and ducted configuration had similar maximum strain components, but the mean strain was lower for the ducted cases at advance coefficient values between -0.2 and -0.7.

Administrative Information

This work was performed at the Naval Surface Warfare Center, Carderock Division, West Bethesda, MD 20817 and was sponsored by the Office of Naval Research under the direction of Dr. Ki-Han Kim and Code 5080. The Project Leader is Dr. Stuart Jessup of the Hydromechanics Division (Code 5030). Work was performed under work unit numbers 07-1-5080-442, 06-1-5080-404 and 08-1-5030-101.

Introduction

Crashback is an extreme event and off-design condition. The crashback condition is one of the most complex and challenging propeller operating conditions to analyze. The loads a propeller experiences in crashback are significantly different from the loads in normal ahead operations. The pressure and suction sides as well as the leading and trailing edges are reversed in crashback causing different hydrodynamics and loading. The propeller loading during crashback has a time-average component, but is dominated by large unsteadiness. Part of the unsteadiness is broadband, while a portion of the unsteadiness is at low frequency and can contribute to propeller maneuvering forces. The unsteadiness also results in extreme propeller blade loading conditions which can severely damage the propeller.

Propeller 4381 was tested in crashback in the Naval Surface Warfare Center, Carderock Division's (NSWCCD) 36-inch water tunnel at Carderock, MD. Both open and ducted configurations [1] & [2] were tested. The objective of the experiment was to compare the strain at the root of the blade for the two configurations. The propeller was instrumented with a strain

gauge at the root of the blade to measure blade strain and derived bending moment during crashback. Advance coefficients varying from -1.2 to -0.3 were tested.

Background

During a crashback maneuver, the initial advance coefficient, J, is typically around +1.0, during normal ahead operations. As the crashback transient begins, the propeller is quickly brought to a stop, during which time the advance coefficient increases from a value of +1 to an infinite J. As the propeller RPM begins to reverse, the propeller enters the crashback, or third-quadrant, of the open water chart with an advance coefficient of negative infinity and begins to move towards zero as the ship continues to slow and the RPM is still negative. If the advance coefficient actually reached zero, the vessel would be at a complete stop, typically crashback maneuvers are halted before that occurs.

For full-scale ships the propulsion system has torque limits. The largest reverse power typically cannot be applied until the shafting achieves its full astern RPM. Based on full scale trial data for several vessels, a ship would have slowed down significantly by the time the maximum negative RPM is achieved and typically, the advance coefficient is in the range of -1 to -0.5, where potential flow codes have a been shown to predict realistic loads for the mean hydrodynamic loadings.

Unfortunately, the mean crashback loading is not a sufficient analysis condition to evaluate a propeller design structurally. Strain gage measurements have determined at both model and full scale that the extreme strain at the root can be as much as 2.5 times higher than the mean root strain [1].

The mean root strain has been used as an indicator for extreme stress events for propellers in crashback. However, most failures that have been attributed to crashback have not occurred in the root region. Failures have been observed near the 0.7 to 0.8 radius, where higher stresses than those occurring at the root may occur. Since strain at the root is easier to measure, that is the region where most data is currently available.

The crashback condition is dominated by the interaction of the free stream flow field with strong recirculation driven by the local propeller-induced velocity. The local propeller-induced velocity pushes the fluid against the incoming free stream flow, shown in Figure 1. The vortex ring created in this condition is unsteady even in the idealized conditions of a water tunnel. Extreme flow unsteadiness and the varying degrees of blade surface flow separation make prediction of individual blade forces extremely difficult.

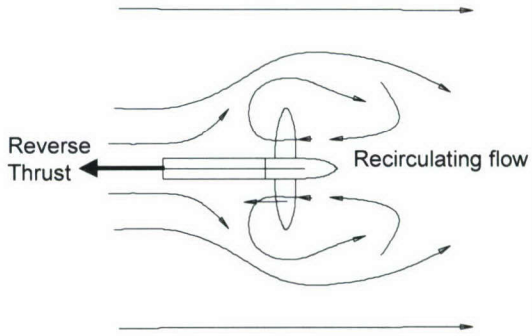

Figure 1. Flow during crashback conditions.

The axial momentum of the fluid that is driven upstream by the propeller is reversed a short distance upstream of the rotor. The fluid then passes around the outside of the propulsor where it is then pulled back into the unit. The time average recirculating pattern is shown in Figure 2 for research Propeller 4381 operating in an open and ducted configuration.

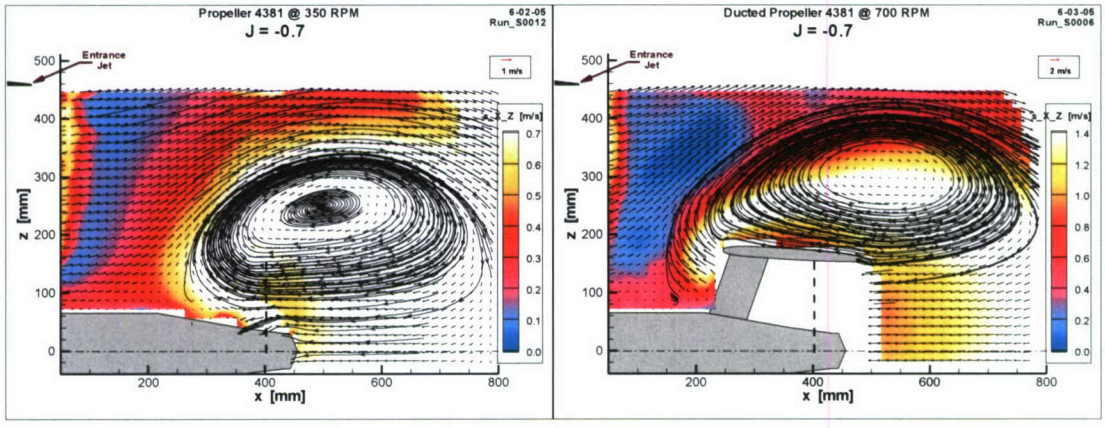

Figure 2. Recirculating flow patterns for Propeller 4381 in the open and ducted configurations at J=-0.7. ([1])

Previous Work

The crashback maneuver has been studied fairly extensively over the past decade. The first flow measurements were performed by Jiang et al [3] , in which PIV measurements were used to relate flow features with measured unsteady shaft forces. This work revealed the presence of a ring vortex structure and its unsteadiness. In particular, the ring vortex was observed to undergo low frequency shedding unrelated to the propeller rotation rate.

Later, Jessup et al [1] supported these findings with a comprehensive set of Particle Image Velocimetry (PIV) and Laser Doppler Velocimetry (LDV) measurements. CFD efforts using Reynolds-averaged Navier-Stokes (RANS) include Chen [4] and Davoudzadeh et al [5]. Chen [4] used RANS to simulate crashback on Propeller 4381. These computations over predicted the

forces in comparison with experimental open water data, and only included modeling of a single blade passage, assuming blade periodic flow. Chen concluded that cavitation was responsible for this discrepancy.

Davoudzadeh et al [5] used RANS to simulate flow over the entire submarine body and propeller during crashback. An unsteady vortex ring was noted, but a comparison with experimental data was not provided. More recently, Vyoshlid and Mahesh [6] & [7] modeled crashback loads using large eddy simulations (LES) for both a full propeller model and an actuator disk model.

Previous tests in the 36-inch water tunnel have been conducted using PIV, LDV, dynomometers, and strain gauges. Results from these tests can be found in Jessup et al. [1] and [2].

Previous Thrust and Torque Data

Figure 3 shows the thrust and the torque coefficients measured for Propeller 4381 from an open water tow tank conducted in 1971*, for all four quadrants of operation. The inflections in the KT and KQ curves in both crashback and crashahead have been associated with large unsteadiness. The early measurements were simple time averages, but did show scatter in these regions.

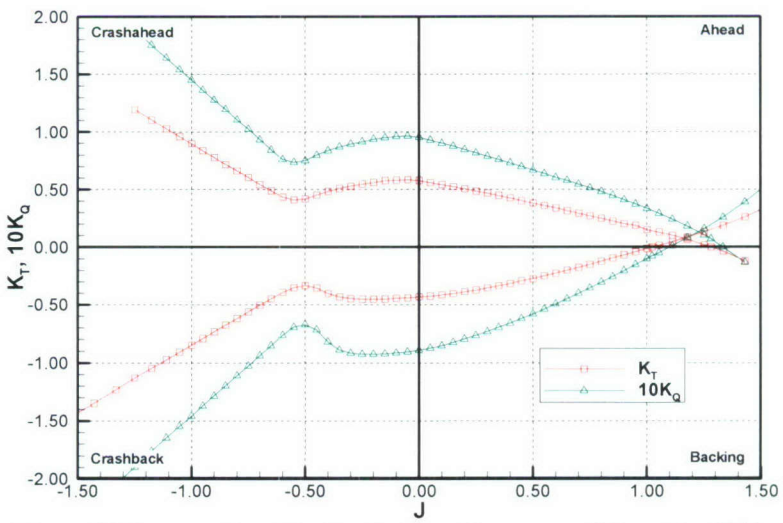

Figure 3. Four quadrant towing tank performance of Propeller 4381.

Jessup et al. ([1] & [2]) presented shaft thrust and torque measurements verses advance coefficient for Propeller 4381 in the 36-inch water tunnel. The 2004 measurements used the

* NSWCCD Technical Report of limited distribution

existing shaft dynamometer at a small fraction of its full capacity, with no corrections for the hub and shaft tares. More recent data shown in Figure 4 represent the best load measurements obtained using an in-hub dynamometer [1]. The load difference between the tow tank and water tunnel results when operating in crashback is not fully understood. Differences could be due to the presence of an upstream shaft in the water tunnel, the fairwater and the downstream shaft in the open water test and a difference in shaft diameter between the two tests. Additionally, there is potentially a tunnel effect due to the close proximity of the ring vortex structure to the tunnel nozzle shear layer, as seen in later PIV measurements [2] and Figure 1.

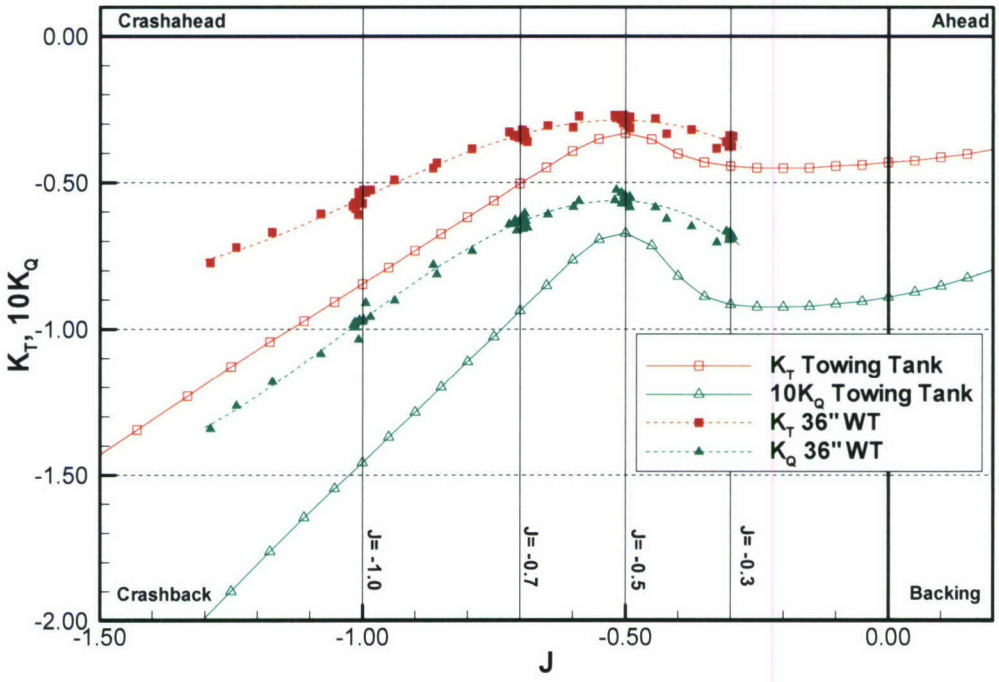

Figure 4. Crashback quadrant data for Propeller 4381 in the towing tank and in the 36-inch water tunnel.

Experimental Set-Up

The experiment was designed to investigate the principle strain at the root of a single blade of Propeller 4381 and the differences between the open and ducted configurations. A range of advance coefficients from -1.2 to -0.3 were run for the crashback conditions and 0.2 to 1.0 for the ahead condition. The advance coefficient, J, is defined as:

$$J = \frac{V}{nD} \tag{1}$$

where V is the tunnel speed, n is the rotational speed of propeller, and D is the diameter. To achieve the variation in advance coefficient the propeller rotational speed was held constant at 700 RPM and the tunnel velocity was varied.

Test Facility

The experiment was conducted in the 36-inch Variable Pressure Water Tunnel (VPWT). The facility is a vertical plane, closed re-circulating tunnel with resorber, variable-speed, variable-pressure, two interchangeable circular test sections – an open jet and a closed jet, a deaerator, and a filter system. The drive system is made up of a 6.5 ft. (1.98 m) diameter adjustable pitch four-bladed axial flow impeller, capable of a maximum test section velocity of 84.3 ft/s (25.7 m/s) and absolute pressures between 2.0 to 60 psi (14 to 414 kPa). Specifications for the test facility are found in [8].

For this experiment the tunnel pressure was set to 35 psi (241 kPa) at the centerline of the tunnel for all experiments except the cavitation experiments. This pressure was set to prevent cavitation inception. For the cavitation experiments the pressure was varied from 12 psi to 20 psi (82.7 to 144.8 kPa).

Tunnel velocities are estimated from pressure measurements using area ratios between static pressure tap locations in the upstream flow contraction area. The 36-inch VPWT has 3 rings of taps for measurement of static pressure in the tunnel contraction upstream of the test section. Tunnel velocity is normally determined between Ring 3 and Ring 1, as they have the largest area difference and greatest pressure drop. Due to the reverse flow generated by a propeller in crashback the static pressure measurement at Ring 1, or closest to the test section, can include an unknown bias error. For this reason another measurement of velocity between Ring 3 and Ring 2 was also acquired in the data set.

Propeller Characteristics

Propeller 4381 is a 5-bladed aluminum propeller with right hand rotation. It has a diameter of 12 inches (305 mm) and zero rake and skew. The expanded area ratio is 0.726. The thickness section is NACA 66 (DTMB Modified) where a = 0.8 camber. The specified geometry characteristics are provided in Table 1. The nomenclature for Table 1 can be found in the nomenclature on page iv.

A drawing of Propeller 4381 and the test hub configuration are shown in Figure 5. In Figure 5, the hub is shown. This hub is different than the hub used for the open water tests which could be another source of discrepancy between the two results.

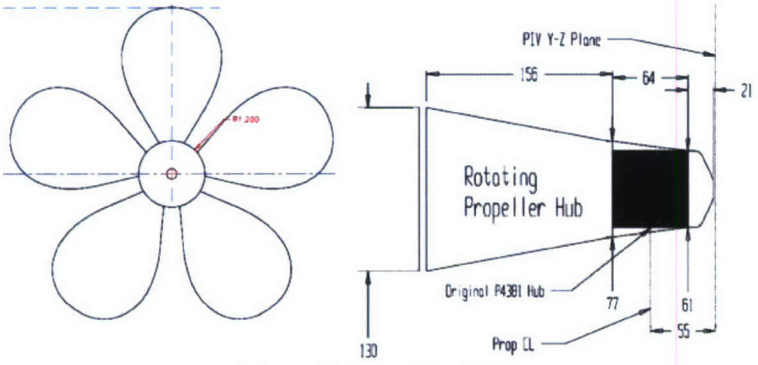

Figure 5. Propeller 4381.

Table 1. Propeller 4381 characteristics

r/R	C/D	t/C	P/D	F/C
0.20	0.174	0.250	1.26	0.0312
0.30	0.228	0.156	1.35	0.0369
0.40	0.275	0.107	1.36	0.0348
0.50	0.313	0.077	1.34	0.0307
0.60	0.338	0.057	1.28	0.0244
0.70	0.348	0.042	1.21	0.0189
0.80	0.334	0.031	1.14	0.0147
0.90	0.281	0.024	1.07	0.0122
0.95	0.219	0.026	1.03	0.0133
0.96	0.202	0.028	1.03	0.0136
0.97	0.180	0.031	1.02	0.0143
0.98	0.153	0.037	1.01	0.0164
0.99	0.115	0.050	1.01	0.0211
1.00	0.000	0.070	1.00	0.0280

Duct Characteristics

To investigate the effect of a duct on the crashback performance, a neutrally loaded duct was designed to fit around Propeller 4381. The duct (P5529) was constructed using SLA plastic with thirteen aligned support vanes ahead of the duct. The ducted configuration is shown in Figure 6. The duct was designed by Thad Michael at NSWCCD using PBD14/MTFLOW ([9]). At the design advance coefficient of 0.89, the duct was designed to contribute no additional propulsor loading. Photographs of the test set-up with the duct installed are shown in Figure 7.

The duct performed as it was designed in that at the design advance coefficient of 0.87, the duct does not affect the loading on the propeller. At lower advance coefficients, the amount of

rotor thrust and torque is reduced as would be expected due to the duct limiting the mass flow rate relative to the propeller only case.

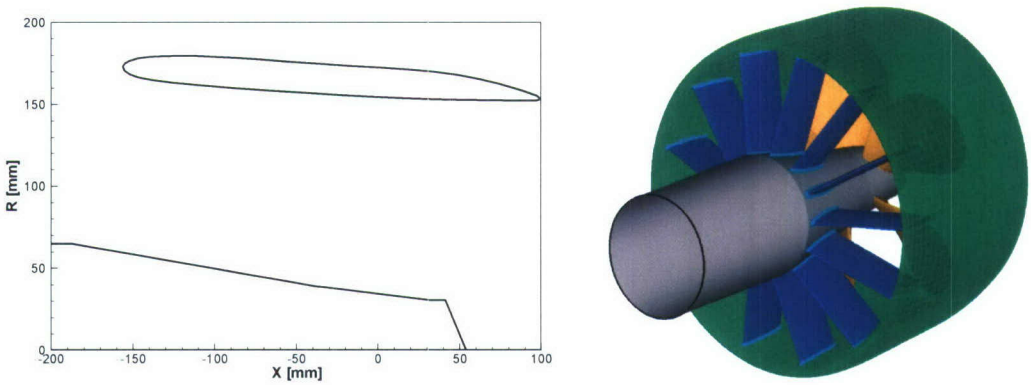

Figure 6. Propeller 4381 in the ducted configuration.

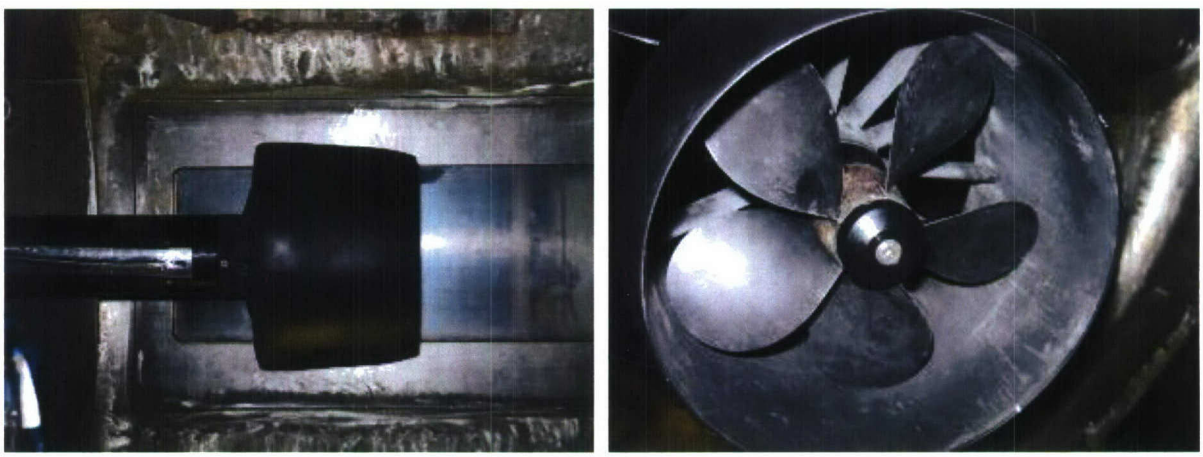

Figure 7. Ducted Configuration for Propeller 4381.

Table 2 gives the geometry for the duct. X equals zero is the propeller plane for the duct. More information is about the duct configuration is available in Appendix A.

Table 2. Duct Geometry

x (mm)	R (mm) upper	R (mm) lower
-156.2	172.4	172.4
-152.4	176.4	168.6
-139.7	179.0	165.2
-127.0	179.6	163.4
-114.3	179.6	162.2
-101.6	179.2	161.1
-88.9	178.5	160.0
-76.2	177.7	159.1
-63.5	176.8	158.2
-50.8	175.9	157.4
-38.1	175.0	156.6
-25.4	174.1	155.9
-1.3	173.3	155.2
0.0	172.5	154.6
12.7	171.7	154.1
25.4	170.7	153.6
38.1	169.4	153.2
50.8	167.6	152.9
63.5	165.1	152.7
76.2	162.0	152.5
88.9	158.2	152.4
98.9	153.2	153.2

Strain Gages

The strain gauge was mounted at 35% of the radius, near the root of the blade on the suction side (upstream facing) in ahead operations. A picture of the strain gage mounted on the propeller is provided in Figure 8. The strain gages were Vishay Micro-Measurements type WA-06-120WR-350 with a quarter wheatstone bridge configuration in three directions, 0°, 45°, and 90°.

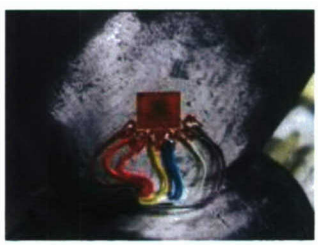

Figure 8. Strain Gauge mounted at the root of the blade.

Initially the blade was instrumented with two strain gauges, one at 30% radius and one at 75% radius. The propeller was installed and tested in this configuration. Two problems were seen with this test set-up. The first was a small crack in the wiring allowed water to get into the system and cause a grounding problem. The electrical zero for the strain gauges varied with the water in the system.

The second problem with the initial instrumentation installation was the potting compound used to waterproof the strain gauges. The potting compound was applied thickly along the mid-chord of the blade from the root to approximately 80% of the radius. The potting compound significantly changed the camber of the suction side of the blade in ahead operations. This compound did not add significant stiffness to the blade, but weighed 0.05 lbs (20.3 grams). After initial testing was done, it was determined that in crashback the potting compound did not significantly change the mean strain on the blade when compared to previous tests, but that the extreme strains were damped out by the application of the potting compound. The thick potting compound and the strain gauge at 75% radius were removed. Once thinner potting compound was applied only at the inner radius the results matched previous tests for the open configuration. The test was then conducted with only one strain gauge at 35% radius.

Data Acquisition System

Measurements were taken with a Dell Optiplex GX270 personal computer running Windows 2000. Data acquisition software and analysis routines were written in LabVIEW v7.1. This collection and analysis code was developed within Code 5800. The PC utilizes a National Instruments PCI-6031E for analog measurements. The PCI-6031E is a 64 channel, 16 bit A/D with a maximum sampling rate of 100 kHz. In order to reduce system noise the board was used in a differential mode limiting the number of analog inputs to 32.

Physical connections to the data acquisition card were made through BNC blocks (NI part numbers BNC2110 and BNC2115). In order to correlate the measured analog data to shaft position the PCI-6031E was synchronized with a digital input board, PCI-DIO-32HS, through the Real Time System Integration (RTSI) bus. The PCI-DIO-32HS was connected to an absolute position encoder in order to record shaft position through a screw terminal connection block (NI part number SCB-68). All data were sampled at a rate of 2000 Hz.

Vishay Model 2310 signal conditioning amplifiers were used to supply the excitation voltage and filter the signals. The filters were set to a low-pass cut-off of 1000 Hz. The gain for the test was set at 1000. The excitation voltage was 10 V. The signal conditioning amplifiers used for the test were 36697, 36726 and 37699. The signal conditioners were zeroed before each set of data runs taken. Electrical zeros were recorded before and after each set of data runs.

Test Matrix

Table 3 shows the test matrix from the crashback testing. Repeat runs were taken at each test condition.

Table 3. Test Matrix.

J	RPM	Tunnel Speed (ft/s)
-1.2	700	12.55
-1.1	700	11.55
-1.0	700	10.55
-0.9	700	9.53
-0.8	700	8.50
-0.7	700	7.45
-0.6	700	6.40
-0.5	700	5.25
-0.4	700	4.17
-0.3	700	3.17
-0.2	700	2.33

Data Reduction

To convert the measured voltage from the Vishay signal conditioning amplifier to strain the following equation was used:

$$\varepsilon = \frac{4V_{out}}{GFNV_{exec}} \tag{2}$$

where V_{out} is the voltage measured, V_{exec} is the excitation voltage, GF is the gage factor, and N is the number of active arms, where N equals one for a quarter bridge. The gage factor for this strain gage was 2.12 at 24°C. The average water temperature of the water tunnel for the duration of the testing was 21°C.

The principle strain can be derived from the three strain gage measurements using:

$$\varepsilon_p = \frac{\varepsilon_1 + \varepsilon_3}{2} \pm \sqrt{\frac{(\varepsilon_1 - \varepsilon_2)^2 + (\varepsilon_2 - \varepsilon_3)^2}{2}} \tag{3}$$

Calibration of Strain Gages

Weights varying from 0 to 22.74 lbs (0 to 10.3 kg) were applied normal to the blade at specified points to calibrate the strain gauges. The blade was rotated such that the normal to the blade was vertical. The weight was applied at three locations at 70% radius, 30% (Location B) chord, 50% (Location A) chord and 70% (Location C) chord. The weight was also applied at 90% radius.

The theoretical bending moment was calculated using the force applied times the distance from the strain gauge to the force. The bending moment was calculated with the following equation:

$$Es = \frac{My}{I} \tag{4}$$

The second moment of inertia at 35% radius is 0.0076 in^4 (3.19e-9 m^4) found using the BSTRESS code and the thickness was 0.0036 T/D. Figure 9 shows the results of the experimental analysis plotted against the theoretical results.

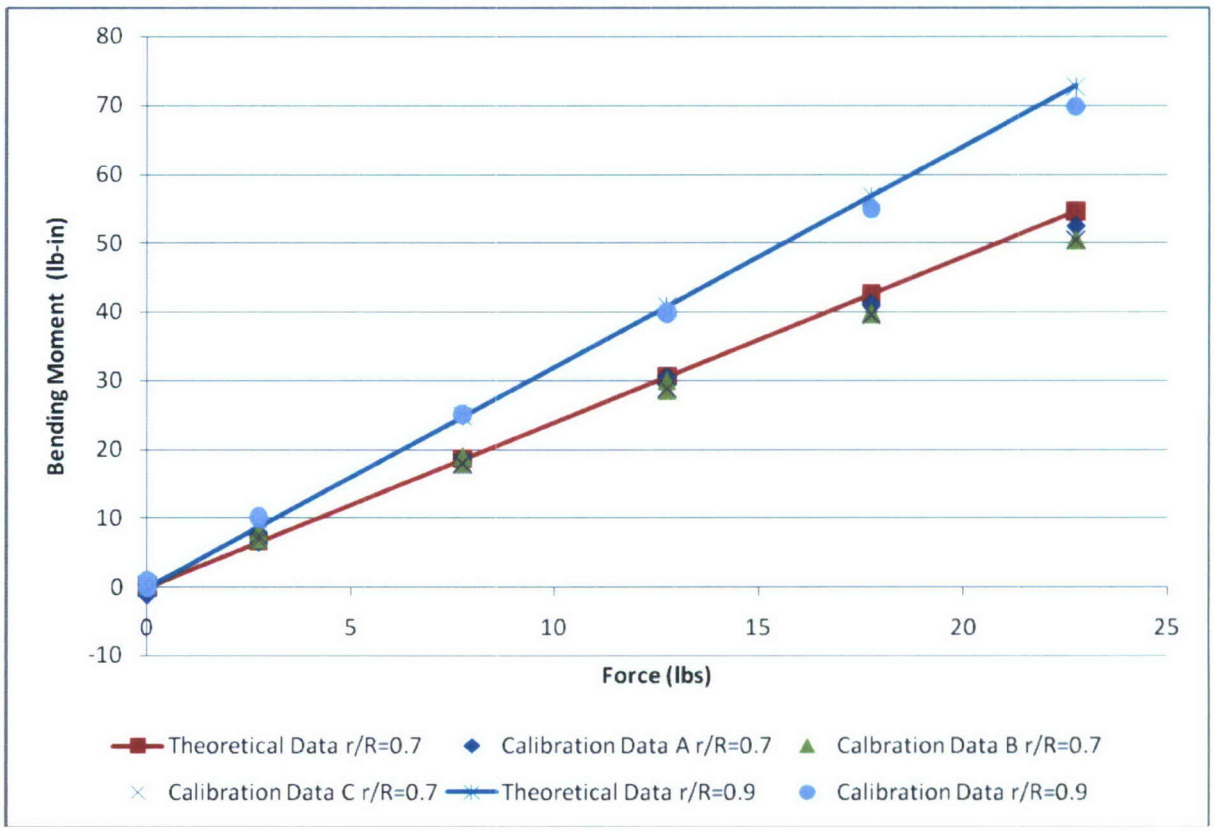

Figure 9. The calibration of the strain gauges versus theoretical calculations

Results and Discussion

Crashback

Figure 10 shows the times series of principle strain. On the left is a full one minute time series. On the right is a view of two seconds of data to show the variation. The time history indicates the extreme unsteady nature of the strain. The peak strains are on the order of three times the mean for some advance coefficients.

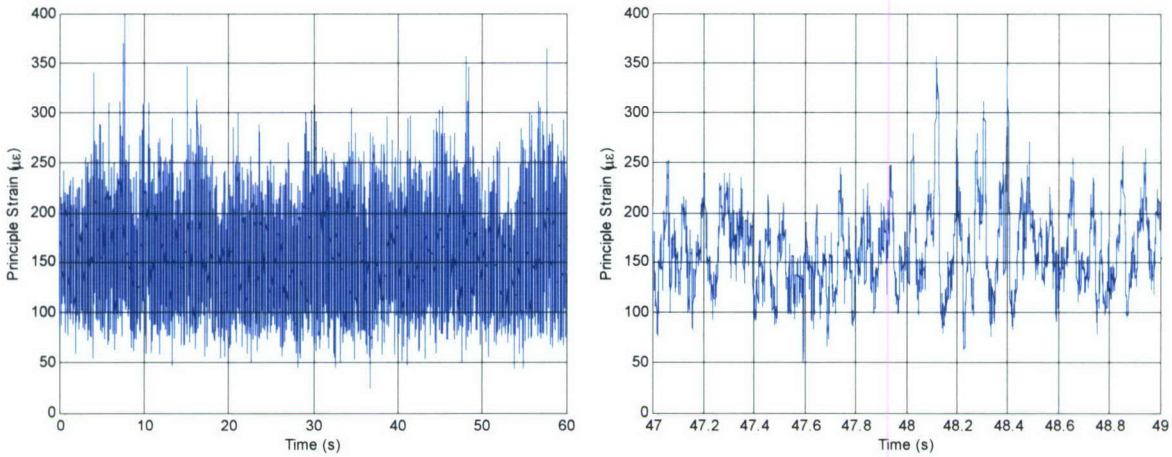

Figure 10. Time series of principle strain.

Figure 11 shows the mean strain at the blade root in crashback for both the open and ducted conditions. From an advance coefficient of -0.7 to -1.2 the open and ducted cases have similar behaviors with the ducted case having a slightly higher magnitude. For an advance coefficient of between -0.7 and -0.2 the strain for the open configuration increases while for the ducted configuration the strain variation is less.

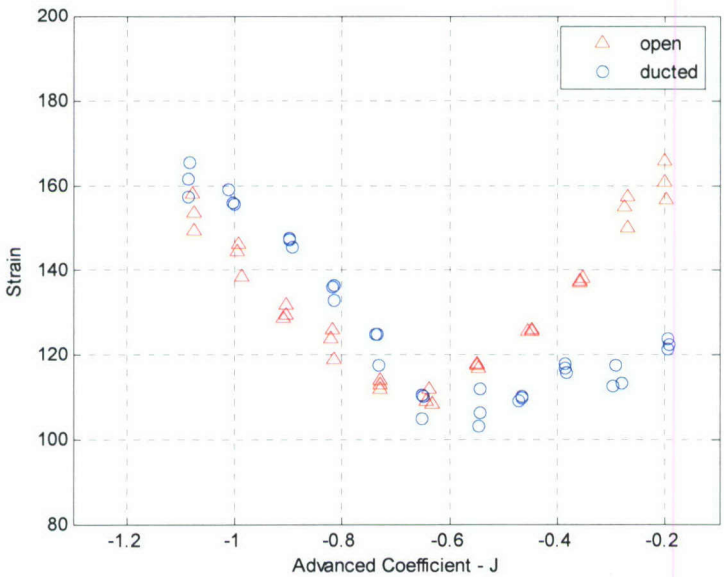

Figure 11. Mean Principle Strain for the open and ducted configurations.

The strain and the bending moment are directly proportional:

$$\varepsilon = \frac{\tau}{E} = \frac{My}{EI} \tag{5}$$

where τ is the stress, E is the Young's modulus, I is the second moment of inertia and y is the distance from the neutral axis. The bending moment is an integration of the pressure difference at either side of the blade at every point on the blade times the distance to that point. Therefore the strain and the thrust at first glance should follow the same trends, if the blade center of pressure is relatively constant. The change in the strain that is seen for the open case, but not for the ducted, could be due to variations in center of pressure; this is discussed later.

The mean strain data from this most recent test in the open configuration is shown compared to strain data taken at the same location in 2006 [2] in Figure 12. Minor differences in the location or orientation of the strain gauge or other experimental differences may explain the difference in the strain.

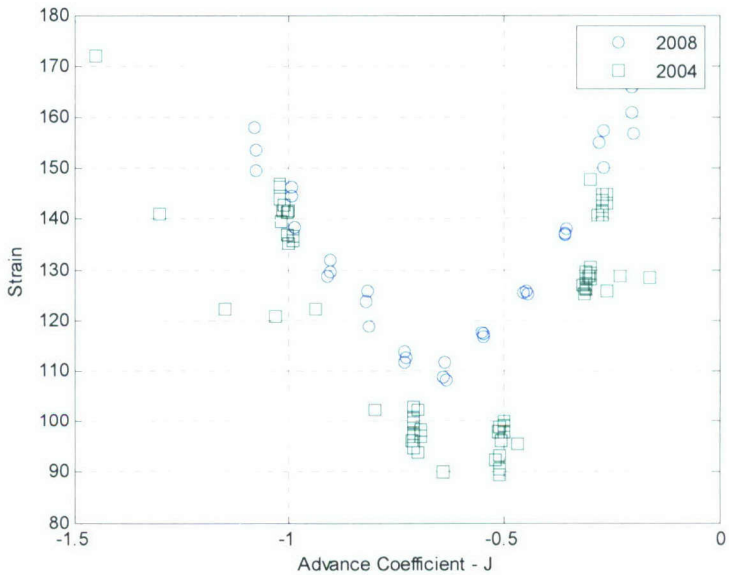

Figure 12. Mean Strain for the open configuration from the 2004 and 2008 tests

The maximum strain was calculated using an average of the ten highest peaks. Figure 13 shows a twenty-second segment of one series with its six highest peaks in that amount of time highlighted with red circles.

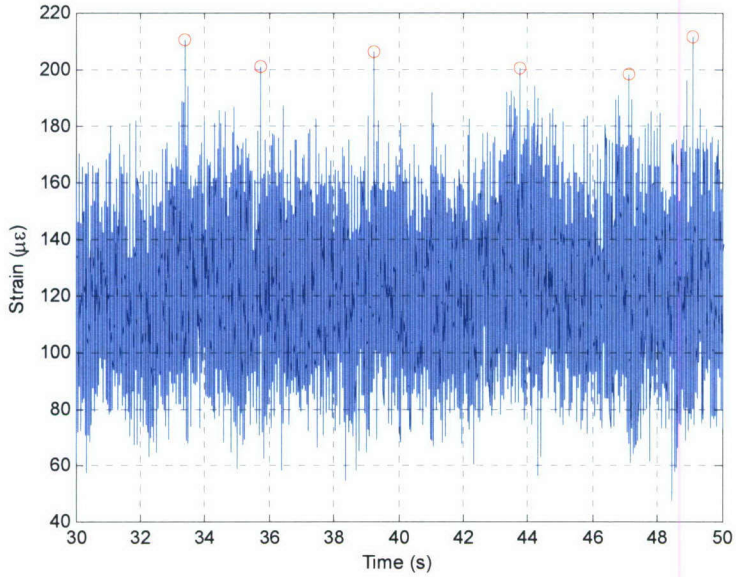

Figure 13. Time series of strain showing the six peak values for the ducted configuration of J = -0.2.

Figure 14 shows the average of the ten highest strains seen for each case (60 second of data). An average of the ten highest was used to prevent one extreme case from skewing the results. Similar results are seen if the average is taken over the three highest points or the twenty highest points. This similarity shows that the peak values for the strain are similar and occur regularly in the time series.

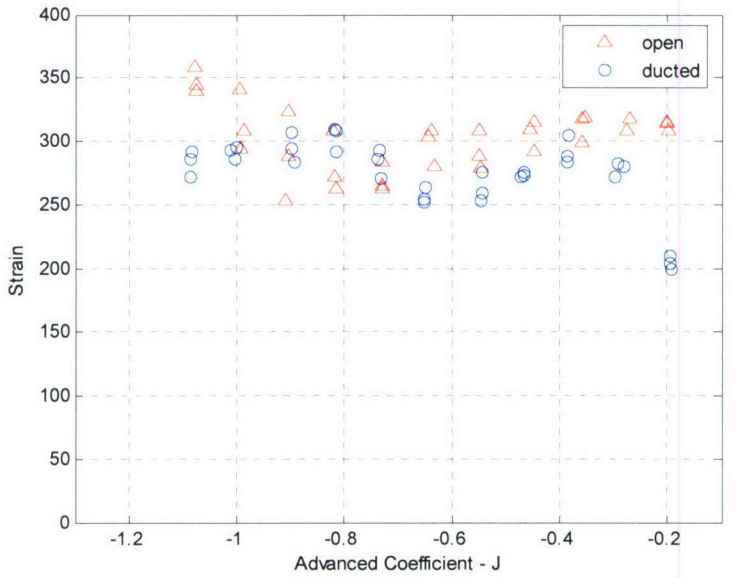

Figure 14. Average of the ten highest maximum strain.

The maximum strain, shown in Figure 14, is consistent across the different advance coefficients and the different configurations. The strain for the ducted configuration is lower than the other data points.

Figure 15 shows the ratio of the average ten highest strains to the mean strain as well as the ratio of the mean plus two and three standard deviations to the mean strain. The ratio of the average ten highest strains to the mean strain is largest at approximately an advance coefficient of -0.7. This increase in the ratio of the highest strain to the mean strain is because the mean strain decreases while the maximum strain appears insensitive to the change in advance coefficient. Figure 16 shows the same ratios from Jessup et al. [2].

Figure 17 shows the same ratio as Figure 15 but for the ducted configuration. The peak in the ratio of maximum strain to mean strain happens at a lower advance coefficient of 0.45 in the ducted configuration. Further investigation is needed to understand why the mean is at a minimum at this value.

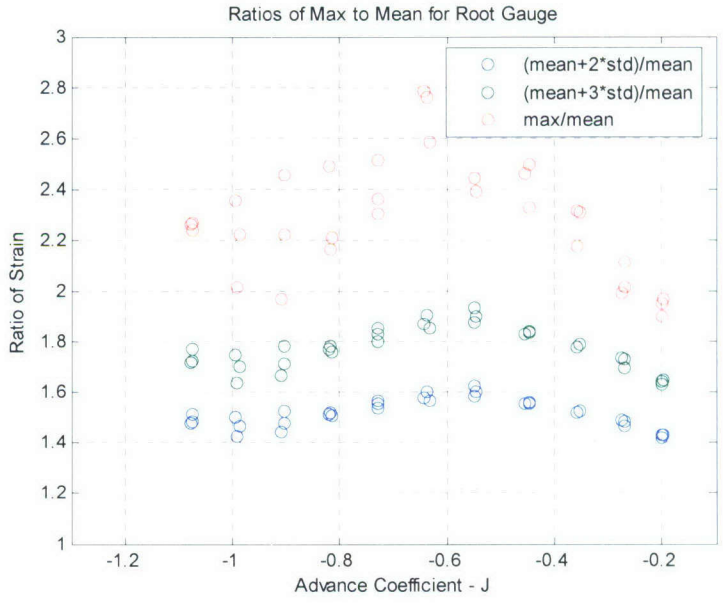

Figure 15. Ratio of the strain for the open configuration.

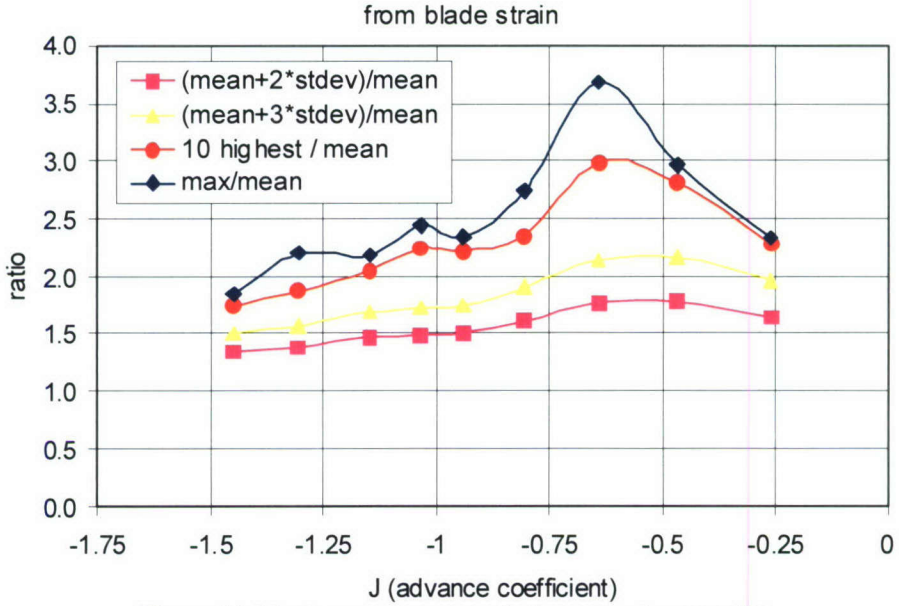

Figure 16. Maximum to mean ratio from previous test [2]

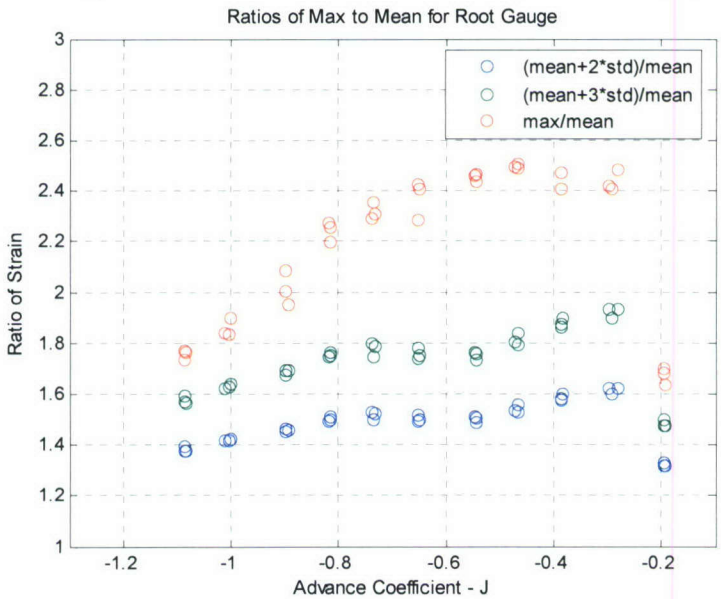

Figure 17. Ratio of strain for the ducted configuration.

The bending moment can be calculated from the strain using the same equation as for the calibration data. Figure 18 and Figure 19 show the mean and average of the ten highest bending moments respectively. The mean bending moments vary from 40 to 60 lb-in (0.46 to 0.70 kg-m), whereas the average of the ten highest bending moments can be as high as 130 lb-in (1.5 kg-m).

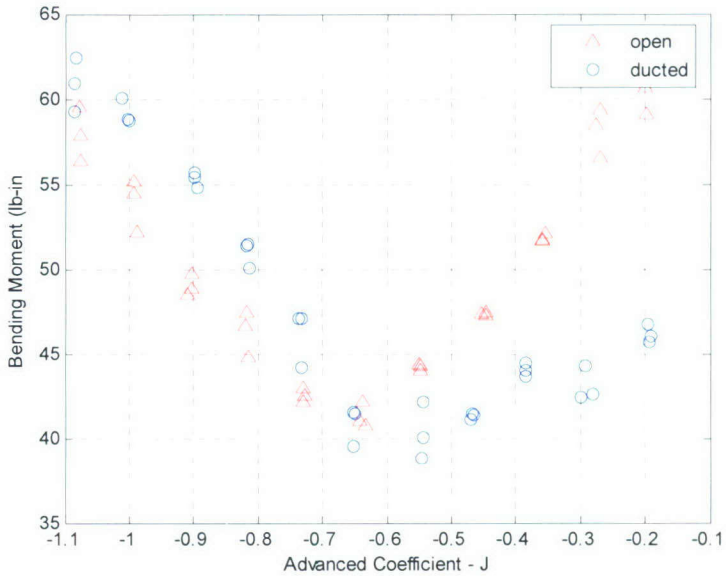

Figure 18. Mean bending moment for the open and ducted configurations.

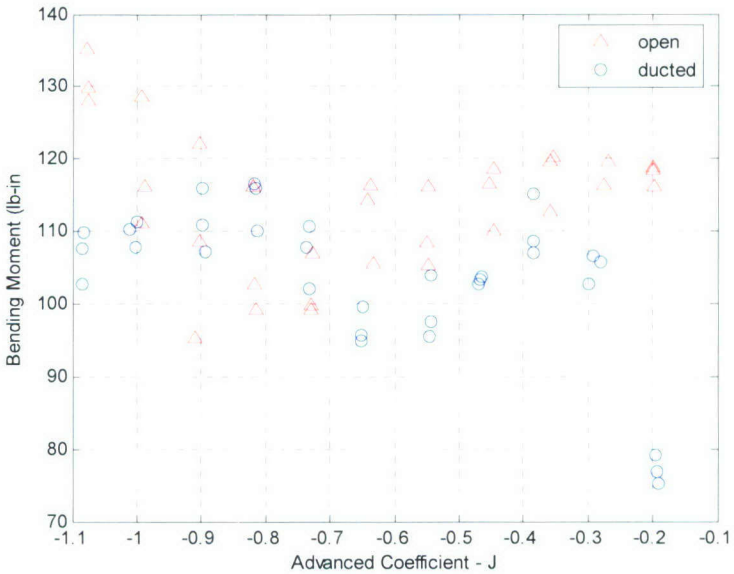

Figure 19. Maximum bending moment for the open and ducted configurations.

Center of Pressure

From the curves shown in Figure 4, a thrust and torque for each blade can be computed using the definition of the thrust and torque coefficients from the water tunnel. Using the torque and thrust, the force, F, excerted on the blade is:

$$F = \sqrt{Y'^2 + \left(\frac{Q}{r}\right)^2} \tag{6}$$

The direction of the force on the blade must be calculated where the angle of the force at the center of pressure (CoP) is:

$$\theta_{CoP} = \tan^{-1}\left(\frac{Tr}{Q}\right) \tag{7}$$

The bending moment then is:

$$M = F\cos(\theta_{r=0.35} - \theta_{CoP}) * d \tag{8}$$

where θ is the pitch angle which is dependant on the radius and d is the distance from the strain gauge to the center of pressure. If a center of pressure is assumed tobe at 0.7R, the results are shown in Figure 20.

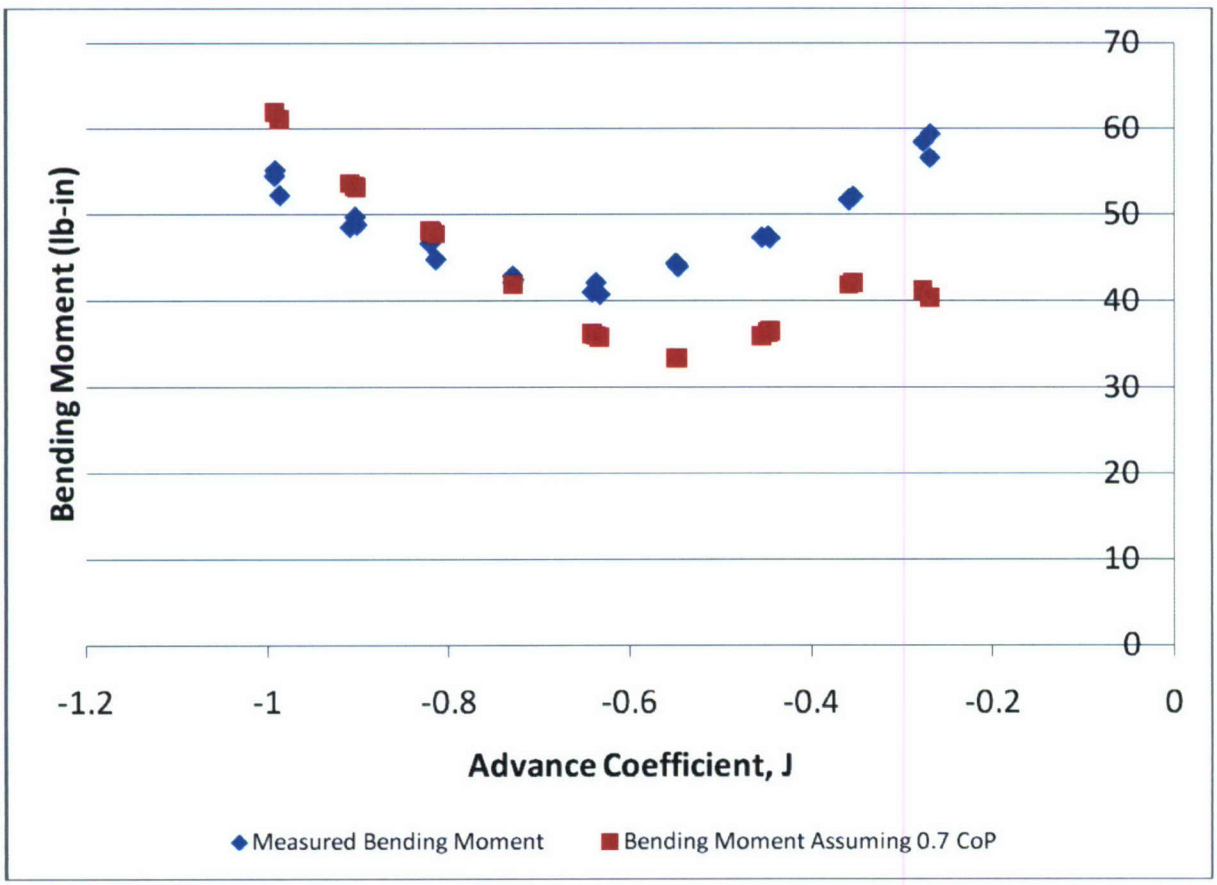

Figure 20. Bending moment calculated assuming a center of pressure of 0.7R.

The distance to the center of pressure can be calculated using the data. The bending moment, M, can be calculated from strain as seen above. Thus the radius of the center, r_{CoP} of pressure is:

$$\frac{EsI}{y} = \sqrt{T^2 + \left(\frac{Q}{r}\right)^2} * \cos\left(\theta_{r=0.85} - \tan^{-1}\left(\frac{Tr}{Q}\right)\right) * (r_{CoP} - r_{r=0.85}) \tag{9}$$

Since this equation is not easily solvable, a minimization function was used to solve for r_{CoP}.The resulting radii of the center of pressure are shown in Figure 21.

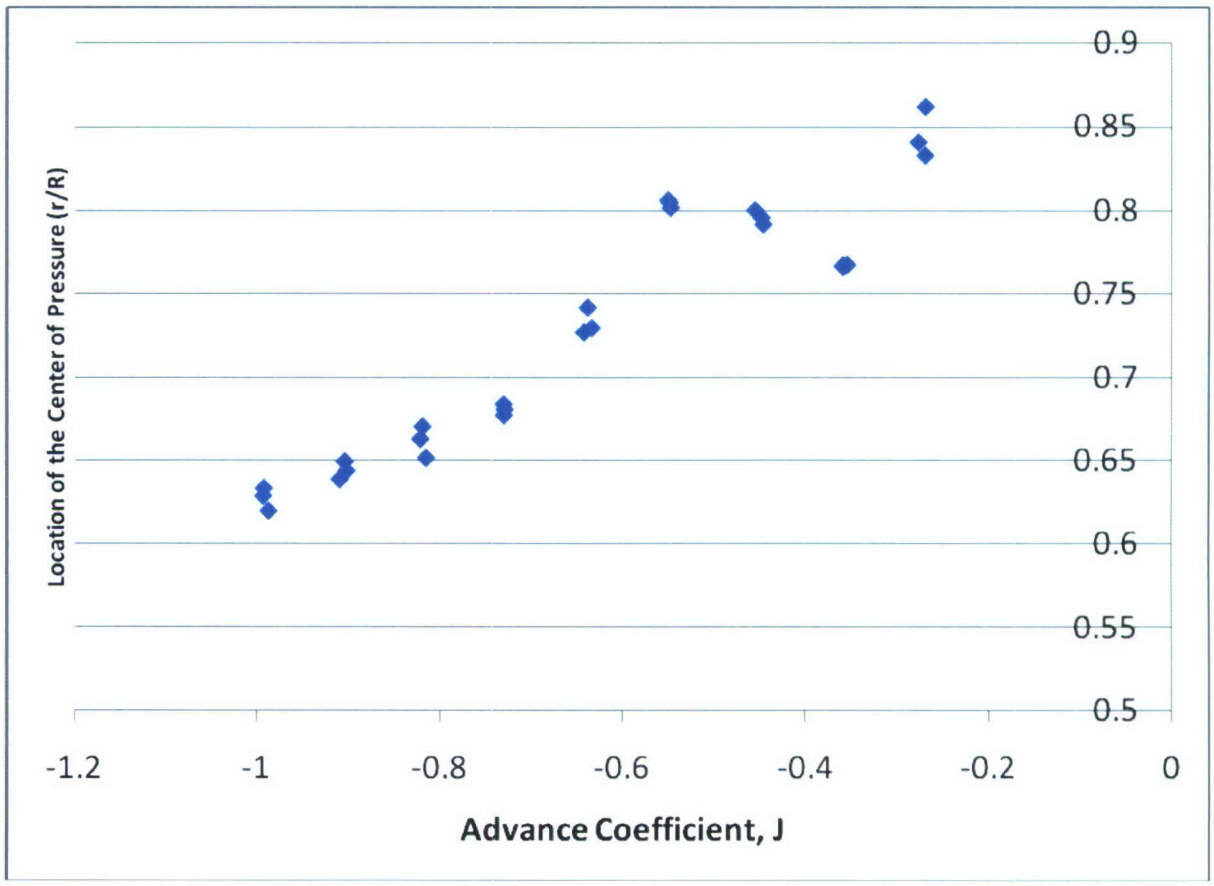

Figure 21. Radius of the center of pressure calculated from bending moment.

The radii of the center of pressure vary from 0.6 to 0.85. At J = -0.3, the trend of increasing radius is unexpected, this may be caused by extrapolation of the thrust and torque curves from the water tunnel.

Frequency of Shedding

Figure 22 and Figure 23 show the average Fast Fourier Transform (FFT) for two different tests at the same advance coefficient for the ducted configuration. The dominant fundamental

frequency is approximately 12 Hz and harmonics of it. For different advance coefficients, the harmonics have different amplitudes. Since the frequency does not change with advance coefficient, the frequency is likely linked to speed of rotation of the propeller and not the tunnel speed. For this experiment the revolutions per minute of the propeller was held constant while the tunnel speed was changed to change the advance coefficient. There was no difference in the frequency content with and without the duct.

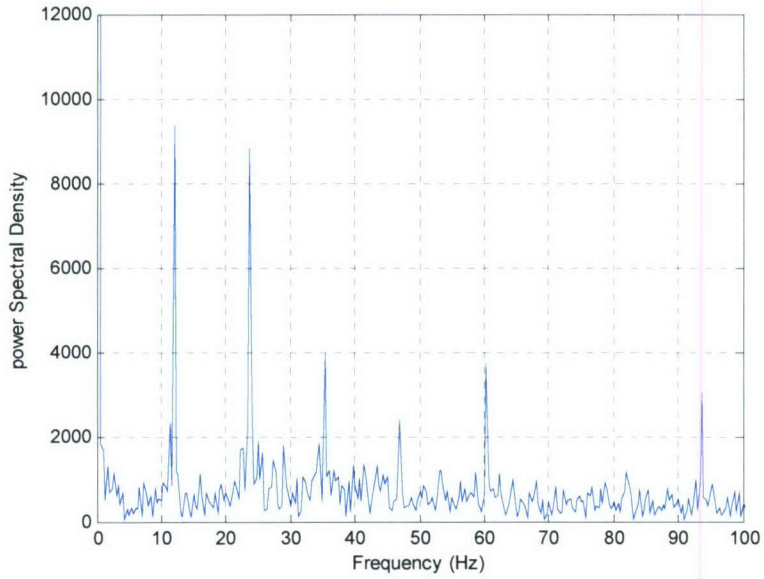

Figure 22. Averaged FFT of principle strain ducted J =-0.2.

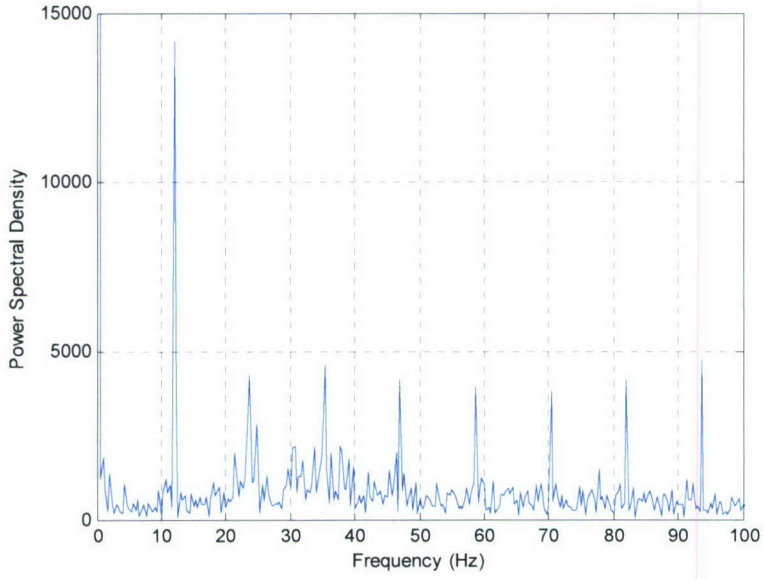

Figure 23. Averaged FFT of principle strain ducted J=-0.2.

The propeller was rotating at 700 RPM for all tests. This speed of rotation corresponds to a shaft rate of 11.667 Hz. In Figures 20 through 22 clear peaks are shown at 11.667 Hz and harmonic multiples of it. These peaks can be caused by imbalances in any part of the system such as in the propeller or the shaft or small hydrodynamic non-uniformities.

Figure 24 shows another averaged FFT from a different advance coefficient. A long frequency peak below 1 Hz is seen here. This frequency has been surmised to be the periodic break-up of the ring vortex seen by Jiang et al. [3] and Jessup et. al. [2].

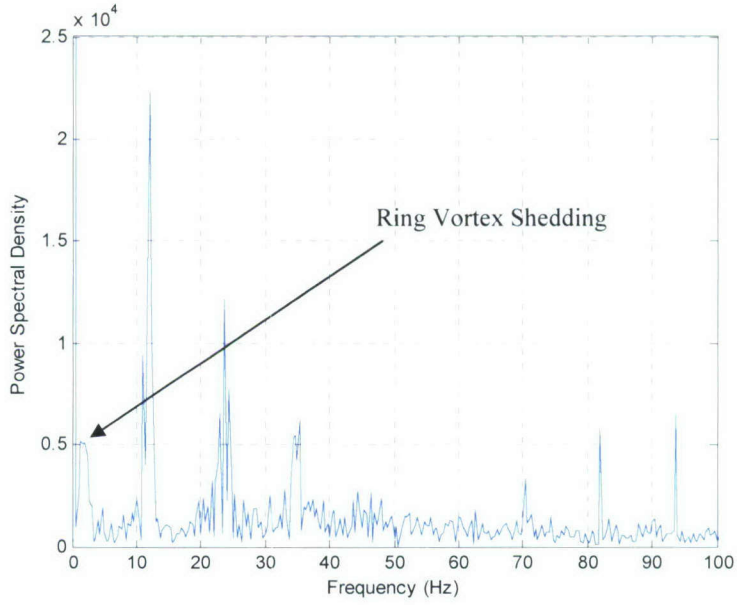

Figure 24. Averaged FFT of principle strain ducted J=-0.3.

Ahead Results and Discussion

The same configuration for both the open and ducted configurations was tested in the ahead condition. The advance coefficient, J, was varied from 0.2 to 1.0. The results are shown in Figure 25. The strain shows the same trend as the first quadrant data in Figure 3 with generally decreasing amplitude with increasing advance coefficient. The duct was designed such that the shaft thrust was equivalent at the design condition of J = 0.87. At a J of approximately 0.82 the open and ducted configurations have similar strain. The strain for the ducted configuration appears to increase at advance coefficients greater than the design condition.

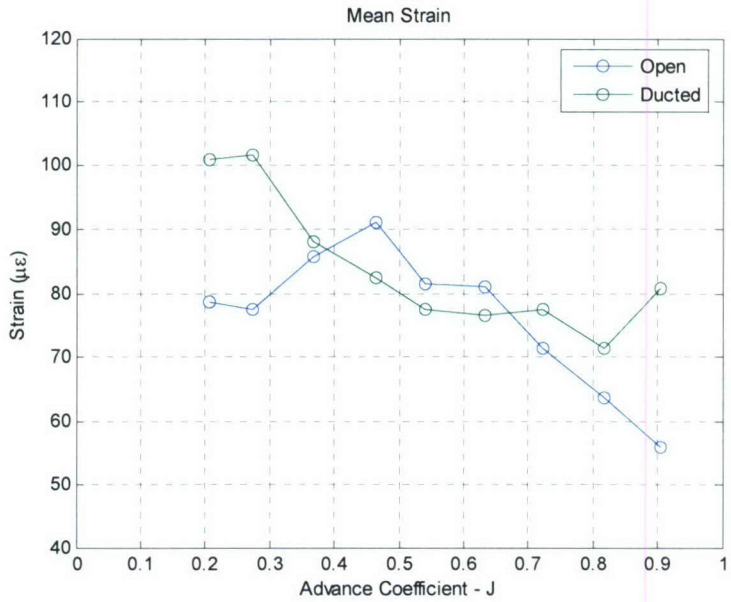

Figure 25. Mean strain of Propeller 4381 in the ahead condition.

Cavitation Tests

Additionally the propeller was tested at reduced pressures to produce cavitation. Advance coefficients of -1.0, -0.7, -0.5 and -0.3 were run in pressures that varied from 12 psi to 25 psi (83 kPa to 172 kPa). At pressure of 20 psi and 25 psi, no significant cavitation was observed. Images of Propeller 4381 at an advance coefficient of -0.7 and a $\sigma = 12$ are shown in Figure 26.

Cavitation can be clearly seen at the tip and on the hydrodynamic leading edge. These results were typical for this low pressure. The increase in pressure decreased the amount of cavitation. Increasing the advance coefficient also increases the cavitation. At an advance coefficient of 0.3 and pressures of 15 and 12 psi (103 and 83 kPa), the air in the tunnel significantly reduced the visibility of the cavitation.

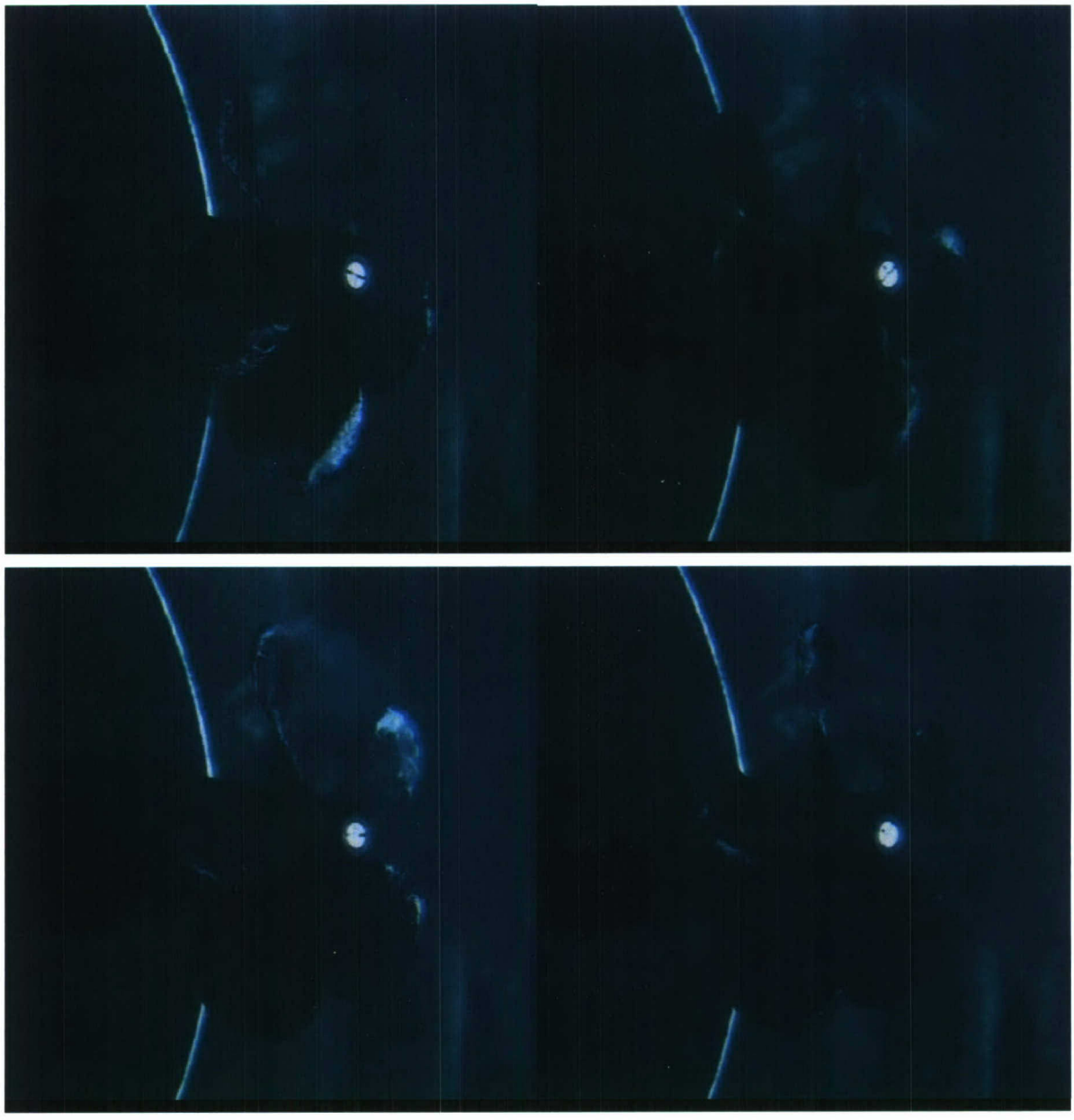

Figure 26. Images of Propeller 4381 cavitating at J=-0.7 and a σ=12.

Conclusions

The experiment measured the strain at the root of a blade of Propeller 4381 undergoing crashback. The test compared the same propeller in an open and ducted configuration. For advance coefficients of -1.2 to -0.7 the mean and maximum strains were similar for both the open and ducted configurations. For advance coefficients of -0.7 to -0.2 the maximum strains were similar for the open and ducted configurations, but the ducted configuration had a lower mean strain. The maximum strains were up to 2.5 times the mean strains seen at the root of the blade. The center of pressure derived from the bending moment was between 0.6R and 0.8R. The open configuration results are consistent with previous results from Jessup et al.[2].

Acknowledgements

The work described in this report could not have been done without the hard work and dedication of Dr. Martin Donnelly, Mr. David Burroughs, Mr. David Bochinski, Mr. David J. Grant, Ms. Nikia Mast, Mr. Joshua Burton, Mr. Patrick McGrail, and Mr. David Brown. Their effort and expertise in instrumentation, installation, and operations are much appreciated.

THIS PAGE INTENTIONALLY LEFT BLANK

References

[1] Jessup, S., Chesnakas, C., Fry, D., Donnelly, M., Black, S., and Park, J., "Propeller Performance at Extreme Off Design Conditions", 25th ONR Symposium on Naval Hydrodynamics, St. John's Newfoundland and Labrador, Canada, 8-13 August 2004.

[2] Jessup, S., Fry, D., and Donnelly, M., "Unsteady Propeller Performance in Crashback Condition With and Without a Duct," 26th Symposium on Naval Hydrodynamics, Rome, Italy 17-22 September, 2006.

[3] Jiang, C.W., Dong, R.R., Liu, H.L. and Chang, M.S., "24-inch Water Tunnel flow Field Measurements During Propeller Crashback," 21st ONR Symposium on Naval Hydrodynamics, 1996, Trondheim, Norway, pp. 136-146, 1996.

[4] Chen, B., "Computational Fluid Dynamics of Four-Quadrant Marine Propeller Flow", Ms.Sc. Thesis, The University of Iowa. 1996.

[5] Davoudzadeh, F., et. al., "Coupled Navier-Stokes and Equations of Motion Simulation of Submarine Maneuvers, Including Crashback," ASME Fluids Engineering Division Summer Meeting, Vancouver, British Columbia, Canada, 1997.

[6] Vyšohlíd, M., Mahesh, K., "Large Eddy Simulation of Crashback in Marine Propellers," AIAA Paper 2006-1415, 2006.

[7] Vysohlid, M. and Mahesh, K., "Understanding Crashback in Marine Propellers Using an Unsteady Actuator Disk Model," 45th AIAA Paper 2007-918, 2007.

[8] Brownell, W. F., "A 36-Inch Variable Pressure Water Tunnel" Navy Department, The David W. Taylor Model Basin Report Number 1052, June 1956.

[9] Renick, D. H., "An Analysis Procedure for Advance Propulsor Design," Masters Thesis, Ocean Engineering Department, Massachusetts Institute of Technology, May 1999

THIS PAGE INTENTIONALLY LEFT BLANK

Appendix A: Duct Configuration Drawings

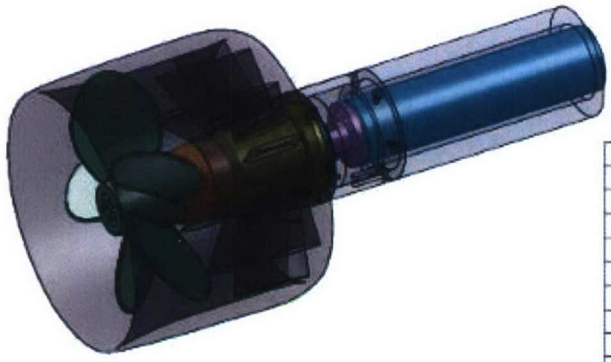

ITEM NO.	DESCRIPTION	QTY.
1	Crashback dyno	1
2	Tunnel and Stator Tube	1
3	Stator Tube Spacer	1
4	Stator Hub	1
5	Tunnel Rotor Shaft	1
6	Rotor Dyno	1
7	Prop Hub	1
8	Rotor Hange	1
9	Rotor Shaft	1
10	Stator	1

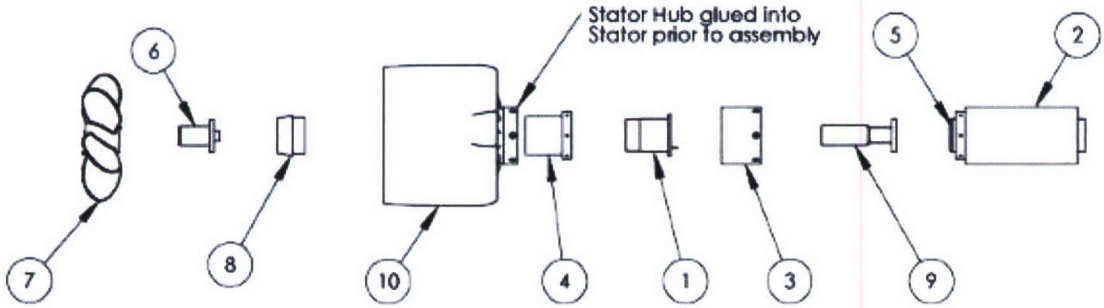

Figure 27. Propeller mounting assembly

THIS PAGE INTENIONALLY LEFT BLANK

INITIAL DISTRIBUTION

				Center Distribution			
Print		Code	Name	Print	PDF	Code	Name
1	ONR				1	3452	Library
	1	331	Kim	-	1	5030	Jessup
1			DTIC	1		5060	Walden
				1		5080	Borda
				-	1	5080	Boswell
				1		5080	Brown
				-	1	5080	Madden
				-	1	5600	Bochinski
				-	1	5600	Etebari
				-	1	5700	Chang
				-	1	5700	Ebert
				2		5800	Files
				-	1	5800	Black
				-	1	5800	Donnelly
				-	1	5800	Fry
				-	1	5800	Fu
				-	1	5800	Lui
				1		5800	Swithenbank
				-	1	6520	Lesar
				-	1	6520	Thurman